ASBMT
American Society for Blood and Marrow Transplantation

Histological Assessment of the Sclerotic Graft-versus-Host Response in the Humanized RAG2$^{-/-}\gamma c^{-/-}$ Mouse Model

Marieke C. H. Hogenes,[1] Suzanne van Dorp,[2] Joyce van Kuik,[1] Filipa R. P. Monteiro,[1] Natalie ter Hoeve,[1] Marijke R. van Dijk,[1] Anton C. Martens,[3,4] Roel A. de Weger[1]

Graft-versus-host disease (GVHD) remains a frequently occurring and difficult-to-treat complication in human allogeneic stem cell transplantation. Murine transplantation models are often used to study and understand the complex pathogenesis of GVHD and to explore new treatment strategies. Although GVHD kinetics may differ in murine and human models, adequate models are essential for identification of the crucial factors responsible for the major pathology in GVHD. We present a detailed description of the specific histological features of a graft-versus-host–induced fibrotic response in xenogeneic RAG2$^{-/-}\gamma c^{-/-}$ mice after total body irradiation and injection with human peripheral blood mononuclear cells. We describe the full morphological features of this reaction, including a detailed analysis of the specific tissue infiltration patterns of the human peripheral blood mononuclear cells. Our data show the development of fibrosis, predominantly near blood vessels, and reveal different cell populations and specific cell migration patterns in the affected organs. The combination of immunohistochemical cell characterization and mRNA expression analysis of both human (donor)- and murine (host)-derived cytokines reveals an interaction between host tissues and donor-derived cells in an entangled cytokine profile, in which both donor- and host-derived cytokines contribute to the formation of fibrosis.

Biol Blood Marrow Transplant 18: 1023-1035 (2012) © 2012 American Society for Blood and Marrow Transplantation

KEY WORDS: Graft-versus-host disease, Mouse model, Histology, Migration patterns

INTRODUCTION

Graft-versus-host disease (GVHD) is a major problem in allogeneic stem cell transplantation, causing late morbidity and mortality [1] and affecting a wide range of organs [2]. One of the difficulties faced in combating GVHD is a poor understanding of the pathophysiology of the syndrome [3]. Steroid therapy and calcineurin inhibitors are currently the most common pharmacologic agents used for treatment and/or prevention of GVHD, although other cells, such as B cells, dendritic cells, macrophages and regulatory T cells (Tregs), might be relevant therapeutic targets as well [4-10].

The study of human GVHD development in vivo has used several different experimental models based on immunodeficient mouse strains, including severe combined immunodeficient (SCID) mice, nonobese diabetic severe immunodeficient (NOD-SCID) mice, and the RAG2$^{-/-}\gamma c^{-/-}$ mice [11-15]. Several xenogeneic mouse models have been reported [15-20], but only a few of these are considered specific GVHD models [15,21-23]. In these mice, human peripheral blood mononuclear cells (huPBMCs), including lymphocytes, are injected into the mice, and the subsequent development of GVHD is studied. To assess the development of the graft-versus-host (GVH) reaction, most studies have focused on the clinical appearance and associated parameters of the mice. However, little is known of the histopathological origin that forms the basis of these "clinical" aspects, and the histological patterns and topographic locations of the different human and murine inflammatory cells has received only minimal attention [15,21,23-25].

In this article, we present a detailed (immuno)histochemical analysis of the localization of human

From the [1]Department of Pathology; [2]Hematology; [3]Cell Biology; and [4]Immunology, University Medical Centre Utrecht, Utrecht, The Netherlands.

Financial disclosure: See Acknowledgments on page 1033.

Correspondence and reprint requests: Roel A. de Weger, PhD, Department of Pathology (H04.312), University Medical Centre Utrecht, Heidelberglaan 100, PO Box 85500, 3508 GA Utrecht, The Netherlands (e-mail: r.deweger@umcutrecht.nl).

Received April 5, 2011; accepted May 1, 2012

1083-8791/$36.00
doi:10.1016/j.bbmt.2012.05.002

immune cells in various organs, as well as the sites of GVH-induced fibrosis in the RAG2$^{-/-}\gamma c^{-/-}$ mouse model. In an attempt to identify the trigger of fibrosis, we used quantitative PCR (qPCR) to measure the mRNA expression of human and murine cytokines in affected tissues. This allows us to examine whether fibrosis is induced by human cytokines directly or by murine cytokines in a reaction to the damage inflicted by human cells.

MATERIALS AND METHODS

Mice and Conditioning Regiments

RAG2$^{-/-}\gamma c^{-/-}$ and Balb/c mice were obtained from the Netherlands Cancer Institute [26]. The mice were bred and maintained in filtertop cages under specified pathogen-free conditions at the Central Animal Laboratory Institute of Utrecht University and were given sterilized food pellets and sterile water ad libitum. The experiment was performed twice.

In each experiment, 10 female mice aged 15-16 weeks received total body irradiation with a single dose of 350 cGy (gamma irradiation from a linear accelerator) and were injected i.v. with huPBMCs the next day. Control groups of 5 RAG2$^{-/-}\gamma c^{-/-}$ mice and 2 Balb/c mice were irradiated but did not receive huPBMCs. Tissues from both control groups were used, to test for specificity of human reagents.

Mice were weighed once a week and sacrificed by cervical dislocation when a loss of >15% of original body weight or severe GVH-associated morbidity was noted. Survival varied between mice, ranging from 29 to 70 days. Experiments were conducted after permission was granted by the local Ethical Committee for Animal Experiments and in accordance with the Dutch law on animal experimentation.

Preparation and Transplantation of huPBMCs

The huPBMCs were prepared as described by van Rijn et al. [15]. In brief, fresh buffy coats were obtained from healthy human volunteers at the blood bank of the University Medical Centre Utrecht, and huPBMCs were isolated using Fiqoll Hypaque (Pharmacia, Uppsala, Sweden) density centrifugation. Cells were washed twice in PBS and resuspended in PBS/0.1% human serum albumin (HSA). Fresh cell suspensions of 0.2 mL containing 15-30 $\times$ 10^6 huPBMCs were injected i.v. into the tail vein without previous ex vivo stimulation, using a different human donor in each experiment.

Histology and Immunohistochemistry

From each mouse, spleen, lungs, liver, ileum and colon, kidneys, skin, heart, and femur were isolated, for a total of 20 morphological analyses per organ (2 experiments with 10 mice each). Each organ was split, with one part frozen and stored in liquid nitrogen and the other part fixed in PBS-buffered formaldehyde (4%). The femur was decalcified with EDTA to enable accurate bone marrow analysis. The formalin-fixed organs were embedded in paraffin and tissue sections were cut into 4-μm sections and mounted on coated slides for staining with H & E for histology and with various primary antibodies for immunohistochemistry (Table 1).

Immunohistochemical staining was performed in a Bond-Max automated immunostainer (Leica Microsystems, Milton Keynes, UK). Slides were pretreated automatically with either citrate, using Bond Epitope Retrieval Solution 1 (AR9961; Leica Microsystems), or EDTA, using Bond Epitope Retrieval Solution 2 (AR9640; Leica Microsystems). Washing steps between each reagent were performed using 1$\times$ Bond Wash Solution (Leica Microsystems). The staining was identified by a polymer-based detection system with diaminobenzidine (DAB) using the Bond Polymer Refine Detection Kit (DS9800; Leica Microsystems). This detection includes incubation with Post Primary for 15 minutes, polymer for 8 minutes, and DAB for 10 minutes. The sections were counterstained with hematoxylin.

For human FoxP3 staining, slides were deparaffinized, washed, and blocked with endogenous peroxidase blocker. Antigen retrieval was performed using citrate pre-treatment, after which slides were washed and incubated with diluted anti-human FoxP3

Table 1. Antibodies Used for Immunohistochemical Detection of Human Cells Injected in RAG2$^{-/-}\gamma c^{-/-}$ Mice

Primary Antibody	Manufacturer	Animal	Monoclonal or Polyclonal	Clone	Lot	Dilution	Pretreatment
Hu-CD2	Novocastra	Mouse	Monoclonal	AB75	127119	1:160	EDTA
Hu-CD4	Monosan Xtra	Mouse	Monoclonal	4B12	247919	1:200	EDTA
Hu-CD8	DakoCytomation	Mouse	Monoclonal	C8/144B	51182	1:200	Citrate
Hu-CD20	DakoCytomation	Mouse	Monoclonal	L26	83	1:400	Citrate
Hu-CD79a	DakoCytomation	Mouse	Monoclonal	JCB117	42791	1:200	Citrate
Hu-CD138	Serotec	Mouse	Monoclonal	B-B4	605	1:1000	Citrate
Hu-κ	DakoCytomation	Rabbit	Polyclonal	-	44399	1:10000	Citrate
Hu-λ	DakoCytomation	Rabbit	Polyclonal	-	120	1:20000	Citrate
Hu-plasmacell	DakoCytomation	Mouse	Monoclonal	VS38C	38925	1:400	EDTA
Hu-CD68	Novocastra	Mouse	Monoclonal	KP1	211708	1:800	Citrate
Hu-FoxP3	EBioscience	Rat	Monoclonal	PCH101	E021753	1:200	Citrate
Mouse-CD68	Hycult Biotech	Rat	Monoclonal	FA-11	4817M21	1:50	None

antibody for 1 hour. After rinsing, slides were incubated for 30 minutes with rabbit anti-rat HRP (Dako, Glostrup, Denmark), diluted at 1:250, and then incubated with Powervision goat anti-rabbit IgG HRP (ImmunoLogic/Klinipath, Duiven, The Netherlands), followed by staining with DAB for 10 minutes after washing with PBS. Slides were counterstained with hematoxylin.

Mouse CD68 staining was performed on frozen tissue sections cut at 8 μm. Slides were fixed in acetone for 10 minutes, then air-dried, rinsed in PBS, and incubated with primary antibody for 1 hour. After rinsing, the slides were fixed in formaldehyde and blocked with endogenous peroxidase blocker before being incubated with a combination of horseradish peroxidase (HRP)-conjugated rabbit anti-mouse antibody (Dako) and 10% mouse serum (Dako) ar a dilution of 1:100. Staining was identified using DAB and counterstained with hematoxylin.

For all monoclonal and polyclonal antibodies used, cross-reactivity against human antigens was tested using both a positive control (human tonsil) and a double-negative control in each run. The latter consisted of a control staining using BALB/c tissue and murine tissue from $RAG2^{-/-}\gamma c^{-/-}$ mice without huPBMCs. In these $RAG2^{-/-}\gamma c^{-/-}$ mice without huPBMCs, a control was run with primary antibody and a control staining using murine tissue with human cells without the primary antibody, to rule out both false- positive staining due to cross-reactivity of the other reagents used and false-negative staining for the primary antibody. Cross-reactivity of anti-murine CD68 was tested in human tonsil tissue.

Slides were assessed for the presence, severity, and location of both fibrosis and cell infiltrates, including the huPBMCs and murine macrophages, by 2 experienced pathologists using light microscopy. The severity of infiltrate with respect to B cells, T helper cells, cytotoxic T cells and plasma cells was scored on a scale of 0 to 4, with 0 indicating no infiltration, 1 indicating sporadic or <5% infiltration, 2 indicating mild infiltration of 5%-25%, 3 indicating moderate infiltration of 25%-50%, or and 4 indicating severe infiltration of >60%. Because the percentage of Tregs in human blood varies from 1%-10%, different thresholds had to be used to score the presence of human Tregs: 0, no infiltration; 1, sporadic infiltration of approximately 1%; 2, mild infiltration of approximately 3%-5%; 3, moderate infiltration of more than 5%-7%; and 4, severe infiltration of more than 7%. Because the percentage of infiltration was evaluated by light microscopy, the scores are somewhat objective. A Krippendorff's κ score of 0.6 was achieved when the 2 pathologists scored individually, but full agreement was achieved by adding the possibility to score intermediately between 2 consecutive scores when doubt persisted and when scores were reevaluated by both pathologists together.

Cytokine Profile Analysis

The cytokine gene expression profile was analyzed by qPCR to measure the amount of human and murine messenger RNA (mRNA) in the murine tissues. Tissue samples were used from mice injected with huPBMCs and from both $RAG2^{-/-}\gamma c^{-/-}$and Balb/c control mice without huPBMCs. RNA was isolated from murine spleen, liver, lung, skin, colon and ileum using the RNeasy Mini Kit (Qiagen, Venlo, The Netherlands), according to the manufacturer's instructions.

For each sample, 3 μg of RNA was incubated with 1 μL of both oligoDT (Promega, Leiden, The Netherlands) and Random Primers (Promega) for 5 minutes at 70°C. Then cDNA was synthesized by adding a mixture of First Strand Buffer 5× (Invitrogen, Breda, The Netherlands), 0.1 M DTT, and 10 mM dNTPs (Invitrogen), followed by incubation for 1 hour at 42°C. The cDNA was stored at −20°C until use [27].

For all cytokines and other gene targets tested, human and mouse specificity was determined by testing the primer–probe combination against mRNA isolated from normal human and murine tissues ($RAG2^{-/-}\gamma c^{-/-}$ and BALB/c mice). Only species-specific predeveloped TaqMan Assays were used (TaqMan Gene Expression Assay; Applied Biosystems, Foster City, CA). The qPCR reactions were run on a LightCycler 480 real-time PCR system (Roche Diagnostics, Lewes, UK). Each sample was run in duplicate, and a negative control was used to exclude contamination. *GAPDH* was used as a reference gene. Relative mRNA quantity was measured using the E-method in the LightCycler 480 software (Roche Diagnostics). In this method, a correction for PCR efficiency is embedded in the calculation of the relative quantity of gene expression.

RESULTS

Clinical Symptoms

All mice injected with human cells (100%) showed development of GVHD symptoms, including significant weight loss, ruffled fur, reduced mobility, skin erythema, and in some cases splenomegaly, as described in other xenogeneic mouse models [15,23,28]. Human chimerism levels in peripheral blood varied from 43%-100% (first experiment) to 5%-51% (second experiment) at the time of death, with consistent weight loss seen in all mice. The pattern of body weight loss was similar to that described by van Rijn et al. [15].

Histological Analysis

After injection of huPBMCs, many organs, including spleen, lungs, liver, skin, bone marrow, gut, and kidneys, were infiltrated with human cells. Because mouse sacrifice was based on clinical criteria, mouse survival varied, ranging from 29 to 70 days. The

mice exhibited varying degrees of fibrosis in the various organs; the longer the survival, the more severe the fibrosis compared with the same organs in mice with a shorter lifespan. Mice with higher human chimerism showed more prominent morphological changes, as described below, although the patterns of fibrosis and infiltrate migration in both experiments were similar and showed clear changes compared with control mice, either as a significant difference or as a trend. Table 2 presents the number of fully examined mice per experiment, mean survival with standard deviation, and mean scores per cell type per organ, with standard deviation and *P* values. A complete description of individual scores of 4 organs in experiment 2 is provided in the Supplementary Data, Table S1. Out of 20 mice, a total of 15 mice (6 from experiment 1 and 9 from experiment 2) could be fully examined. Five mice died from the GVHD and were lost for evaluation because of severe postmortem lytic changes.

Spleen

The spleen contained large amounts of collagenous fibrosis around smaller blood vessels (Figure 1). With longer survival time, the severity of the infiltrate increased concurrently and the distribution of the infiltrate became more diffuse. With more extended infiltration through the tissue, the fibrosis spread in the rest of the parenchyma as well, destroying the entire morphology of the spleen.

Lungs and liver

Fibrosis around blood vessels was observed in the lungs. The fibroses were concentrated around peribronchial blood vessels and to a lesser degree around bronchi and bronchioles when more extensive infiltrate was present (Figure 2). The liver demonstrated periportal fibrosis (Figure 3) lined with plasma cells along the lamina limitans, with some bile duct proliferation.

Skin

Fibrosis was particularly extensive in the skin (Figure 3). The morphology was quite similar to the human sclerodermatous GVH reaction, with a mild lichenoid infiltrate along the epidermal junction, thinning of the epidermal layer, extension of coarse collagen fibers in the dermis at the cost of the underlying subcutaneous fat, and loss of hair follicles. Only a few infiltrating human cells were present.

Bone marrow

The bone marrow showed clear signs of fibrosis, but the cellularity of the marrow was maintained.

Other organs

There were no obvious signs of tissue damage in the gut, in contrast to the human counterpart. Likewise, the kidneys and heart demonstrated no signs of tissue damage, despite the presence of human infiltrating cells (see below for specification).

Morphological Infiltrate Analysis

Immunohistochemical staining revealed no cross-reactivity between species, considering both primary and secondary antibodies, and thus was considered appropriate for determining the topographic location of the different cells in the murine tissue.

As expected, no infiltrating human cells were found in the control RAG2$^{-/-}\gamma c^{-/-}$ mice. Only mouse macrophages were observed in control mice tissues, using anti-mouse CD68. In mice injected with human cells, most of the human cell infiltrate was found in the spleen, lungs, and liver, with little seen in skin, gut, kidney, heart, and bone marrow. The different organs showed typical consistent infiltration patterns, described below. In general, most of the infiltrate concentrated in areas that would normally contain lymphoid tissue in nonimmunodeficient mice and humans, and also around blood vessels. Human macrophages were not found in any organs, but mouse macrophages (mouse CD68$^+$) were found mixed with the human infiltrate, mainly in spleen, lungs, and liver.

Spleen

In spleen, the infiltrating human cells first appeared around blood vessels on day 29 and with longer survival spread diffusely in the parenchyma, with expansion of the infiltrate (Figure 1). The infiltrate consisted of a combination of huCD2$^+$ T cells (predominantly CD8$^+$ cytotoxic T cells [CTLs]) with B cells (huCD20$^+$ and huCD79a$^+$) and a considerable number of plasma cells (huCD138$^+$ and VS38c$^+$). The B cells and plasma cells were polyclonal for hu-λ and hu-κ. The B cells and some plasma cells were usually found around blood vessels in a follicular pattern, in the same areas that demonstrated fibrosis. This site corresponds to the white pulpa zone in nonimmunodeficient species. T cells spread diffusely throughout the parenchyma. Few Tregs (FoxP3$^+$) were detected and those present were scattered throughout the tissue. Murine macrophages (mouse CD68$^+$) were scattered diffusely through the parenchyma (data not shown).

Lungs and liver

In the murine lungs and liver (Figures 2 and 3), B cells and plasma cells were concentrated around blood vessels, with some spread along the bronchi. Mainly larger arteries along the bronchi were surrounded by a B cell infiltrate, closely matching the areas in which fibrosis was detected histologically. T cells were

Table 2. Statistical Analysis of the Immunohistochemical Data

			Fibrosis		T Cells		B Cells		Plasma Cells		Tregs	
	N	Survival, Days, Mean (SD)	Histopathology Score, Mean (SD)	*P* Value	Histopathology Score, Mean (SD)	*P* Value	Histopathology Score, Mean (SD)	*P* Value	Histopathology Score, Mean (SD)	*P* Value	Histopathology Score, Mean (SD)	*P* Value
Spleen												
Exp. 1	6	36.7 (7.2)	0.7 (0.8)	.1028	3.2 (0.4)	.0034	2.0 (0.9)	.0052*	2.3 (1.5)	.0049*	1.2 (0.4)	.0034*
Exp. 2	9	39.5 (14.3)	1.8 (1.2)	.0145*	3.7 (0.5)	.0017	2.4 (1.0)	.0047*	2.1 (1.2)	.0061*	1.2 (1.3)	.0615
Exp.1 vs. exp. 2				.0875		.0769		.2716		.9038		.9017
Liver												
Exp. 1	6	36.7 (7.2)	1.5 (0.8)	.0140*	2.7 (0.5)	.0043*	1.2 (0.4)	.0034*	1.5 (1.0)	.0163*	0.3 (0.8)	.4652
Exp. 2	9	39.5 (14.3)	1.7 (0.7)	.0021*	2.0 (1.2)	.0137*	0.8 (0.7)	.0277*	0.6 (0.5)	.0548	0.6 (0.5)	.0545
Exp.1 vs. exp. 2				.9479		.3268		.2300		.0658		.3074
Lung												
Exp. 1	6	36.7 (7.2)	0.5 (0.5)	.0990	2.7 (0.5)	.0043*	1.2 (0.4)	.0034*	1.3 (0.5)	.0043*	0.5 (0.8)	.2230
Exp. 2	9	39.5 (14.3)	2.1 (1.0)	.0024*	2.7 (0.5)	.0017*	0.8 (0.8)	.0603	0.7 (0.9)	.1114	0.8 (0.4)	.0090*
Exp.1 vs. exp. 2				.0069*		.9429		.2993		.1171		.2880
Skin												
Exp. 1	6	36.7 (7.2)	3.0 (0.9)	.0052*	2.7 (1.0)	.0050*	0.0 (0.0)	†	1.0 (1.2)	.01041	1.0 (1.2)	.1041
Exp. 2	9	39.5 (14.3)	1.8 (0.8)	.0023*	2.2 (1.0)	.0024*	0.0 (0.0)	†	0.0 (0.0)	‡	0.4 (0.7)	.1931
Exp.1 vs. exp. 2				.0322*		.4587		†		.1041		.4224
Colon												
Exp. 1	6	36.7 (7.2)	0.7 (0.8)	.1028	2.3 (0.5)	.0043*	0.0 (0.0)	†	0.0 (0.0)	‡	0.2 (0.4)	.4652
Exp. 2	9	39.5 (14.3)	2.4 (0.5)	.00019	2.7 (1.2)	.0060*	0.0 (0.0)	.5500	0.0 (0.0)	‡	0.1 (0.3)	.5716
Exp.1 vs. exp. 2				.00030*		.2800		.4960		‡		.7768

Mean survival with standard deviation (SD), mean scores with SD and *P* values for histological and immunohistochemical scoring in the most important evaluated organs in experiment 1 (comparing mice injected with huPBMCs and control mice without huPBMCs), experiment 2 (comparing mice injected with huPBMCs and control mice without huPBMCs) and comparing experiments 1 and 2 for differences between the groups of mice with huPBMCs. An example of individual scoring in 4 organs from experiment 2 can be found in Table S1 in Supplementary Data.

**P* value is significant.

†No B cells detected; *t* test not possible.

‡No plasma cells detected; *t* test not possible.

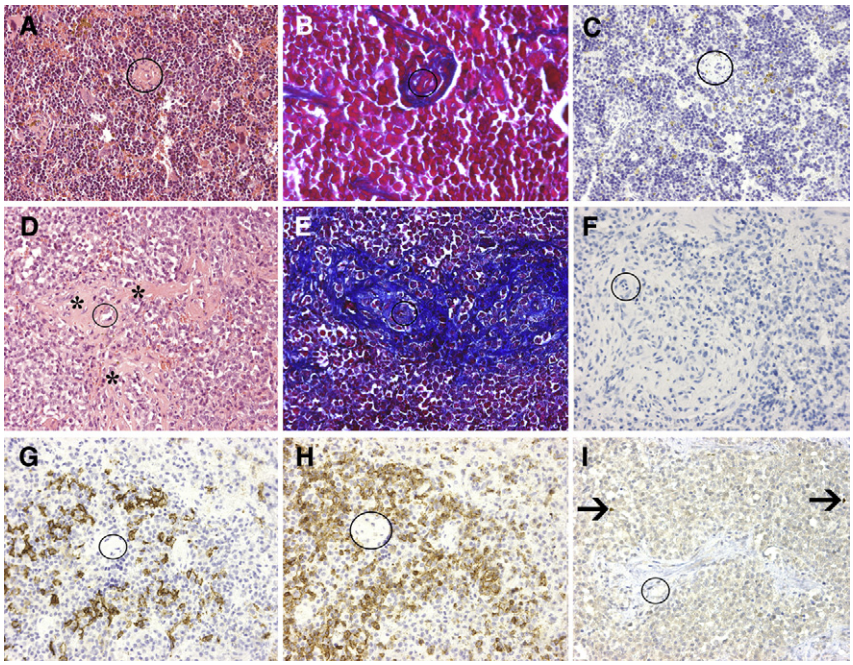

Figure 1. Human infiltrating cells in spleen of RAG2$^{-/-}\gamma c^{-/-}$ mice injected with huPBMCs. Infiltrate analysis of spleen comparing both histological and immunohistochemical stainings of a control mouse and a mouse surviving 45 days after huPBMC injection is shown. The morphology is representative of the observed reaction in a total of 15 examined mice (6 mice in experiment 1 and 9 mice in experiment 2). (A) Normal murine spleen, without human cell infiltrate or fibrosis (H & E staining; original magnification, 20×). (B) Normal murine spleen without human cell infiltrate or fibrosis (AZAN staining; original magnification, 20×; fibrosis score 0). (C) Normal murine spleen, showing no immunohistochemical positivity and no cross-reactivity when staining for human CD2$^+$ T cells (huCD2 staining; original magnification, 20×; T cell score 0). (D) Perivascular fibrosis in spleen in a mouse 45 days after huPBMC injection (H & E staining; original magnification, 20×; fibrosis score 2). (E) Perivascular fibrosis spleen (identical area to that shown in D) showing blue staining of the formed collagenous fibrosis (AZAN staining; original magnification, 20×; fibrosis score 2). (F) HuCD68 cells showing the absence of human macrophages in a mouse injected with huPBMCs (huCD68 staining; original magnification, 20×; macrophage score 0). (G) Follicular/perivascular concentration of human B cells in the spleen after injection with human PBMCs (huCD20 staining; original magnification, 20×; B cell score 2). (H) Diffuse spreading of human T cells in the spleen after injection of human PBMCs (huCD2 staining; original magnification, 20×; T cell score 4). (I) Focal localization of human Tregs with nuclear positive staining for huFoxP3 after injection with human PBMCs (huFoxP3 staining; original magnification, 20×; Treg score 1). A circle indicates localization of capillary blood vessels; asterisk, fibrosis area; arrow, FoxP3$^+$ Tregs.

distributed throughout the alveolar septae but were also detected mixed with B cells perivascularly. Many murine macrophages were found in the alveolar spaces (Figure 2).

In the liver, the major sites of infiltration were the periportal and pericentral area. B cells were located around vessels, mainly the periportally and pericentrally located arteries (Figure 3). These areas closely matched the areas of fibrosis in the previous histological analysis. T cells were located in the hepatic sinuses, along with an increased number of murine CD68$^+$ macrophages. There was a mixture of T helper cells (CD4$^+$) and CTLs (CD8$^+$) in both lungs and liver, with no predilection for either cell type. Only a few Tregs were detected, not confined to specific areas in the tissue.

Skin

The skin showed only small numbers of infiltrating T cells (predominantly CD8$^+$ CTLs), located subepidermally and surrounding hair follicles. Sporadically a single Treg was detected, but no B cells or plasma cells were identified (Figure 3). There was no correlation between the location of the previously described fibrosis and the cellular infiltrate.

Gut

The gut (including colon and ileum) showed infiltration of T cells with scattered Tregs in the submucosa, in areas where one would normally expect the mucosal-associated lymphoid tissue in nonimmunodeficient species. In the colon, the infiltrate consisted mainly of T helper cells (CD4$^+$). In the ileum there was a relatively large amount of CTLs (CD8$^+$). As in the skin, no B cells or plasma cells were observed.

Kidneys

The kidneys contained a mild infiltrate of T cells, with a combination of CTLs (CD8$^+$) and T helper cells (CD4$^+$), particularly around blood vessels and sometimes near or in glomeruli.

Heart

In the heart, just a few T cells were detected within major heart valves, but these could not be further specified. No human cells were found in the myocardium.

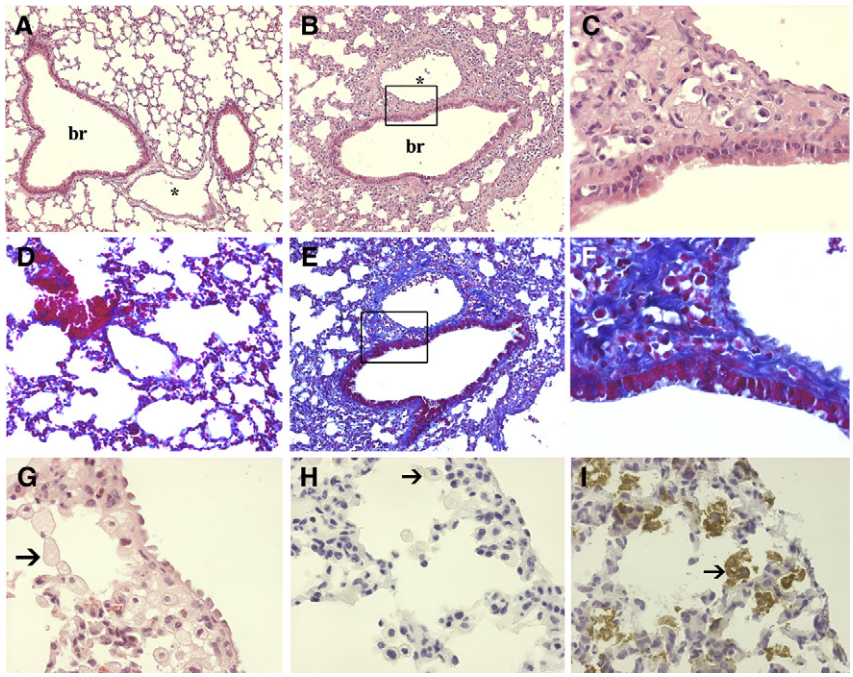

Figure 2. Histological and immunohistochemical analysis of infiltrating human cells in RAG2$^{-/-}\gamma c^{-/-}$ lungs. Infiltrate analysis of the lungs comparing a control mouse and a mouse from experiment 1, surviving 45 days after huPBMC injection, is shown. The morphology is representative of the observed pattern in a total of 15 examined mice (6 mice in experiment 1 and 9 mice in experiment 2). (A) Normal murine lung showing thin alveolar septae around bronchi and blood vessels (H & E staining; original magnification, 10×; fibrosis score 0). (B) Lung after injection with human PBMCs, showing perivascular and peribronchial fibrosis and cell infiltration with hypercellular alveolar septae 45 days after huPBMC injection (H & E staining; original magnification 10×; fibrosis score 1). (C) Detail from (B) (inset) showing plasma cells in the area of fibrosis (H & E staining; original magnification 40×; plasma cell score 1). (D) Normal lung showing thin alveolar septae without extensive fibrosis around bronchi or vessels (AZAN staining; original magnification, 10×; fibrosis score 0). (E) and (F) Same areas as in (B) and (C) respectively, in AZAN staining, with blue staining of the collagenous fibrosis (E, original magnification 10×; (F) detail from (E) inset; original magnification, 40×; fibrosis score 1). (G) Foamy alveolar macrophages after injection with huPBMCs (H & E staining; original magnification, 40×). (H) The macrophages do not show human CD68 positivity (huCD68; original magnification, 40×; identical area to that shown in H). (I) Positive staining of macrophages for mouse CD68 confirms murine origin (mouse CD68; original magnification, 40×; identical area to that shown in H). Br, bronchus. An asterisk denotes the peribronchial artery; an arrow, foamy alveolar bronchophages. The square is a detail of the area shown in (C) (corresponding to the square in B) and (F) (corresponding to the square in D).

Bone marrow

The cellular bone marrow of the mice showed only few scattered human cells, consisting mainly of T cells (predominantly CD8$^+$) and sporadic plasma cells, along with a few murine macrophages. No human B cells and virtually no Tregs were present. The increase in reticulin fibers could not be related to a specific human cell type in these areas.

Cytokine Profile

qPCR revealed high RNA levels for the human cytokines transforming growth factor (TGF)-β and especially IFN-γ in all organs tested. The calculated relative quantities (RQ) for TGF-β were particularly high in the liver compared with the spleen, lung, skin, and gut (Figure 4). The data showed a mixture of infiltrate in all affected organs, containing RNA for cytotoxic T cells (CD8) and T helper cells (CD4), including Th1 cells (Tbet) and Th2 cells (GATA3), with some variation in the amounts of these different cell types among organs. Th17 cells (RORC) were also present, but Tregs (Foxp3) were found only in the spleen, lungs, and skin (Figure 5). The detected variation in cell types based on qPCR markers was well correlated with the previous immunohistochemical results. The expression of CXCR4 explained the attraction for lymphocytes to these organs. Furthermore, only mouse-derived CD68$^+$ macrophages were detected. Threshold cycle values for human CD68 were very low, implicating a paucity of human macrophages (Figure 4).

No fibrotic or other inflammatory-related cytokines, such as FGF2, PDGF, or EGF (data not shown), or BMP4 or CTGF mRNA of human origin were detected (Figure 4). Expression of human RNA for PAI was low in lung and very low in skin (data not shown); however, high levels of murine CTGF were found in the lung and skin (Figure 4). High levels of murine TGF-β were observed as well, but this appears to be unrelated to human PBMC injection, given that the level of murine TGF-β in control RAG2$^{-/-}\gamma c^{-/-}$mice was as high or even higher. Murine BMP4 was recovered at low levels from lung, skin, colon, and ileum, and was detected in both test and control mice.

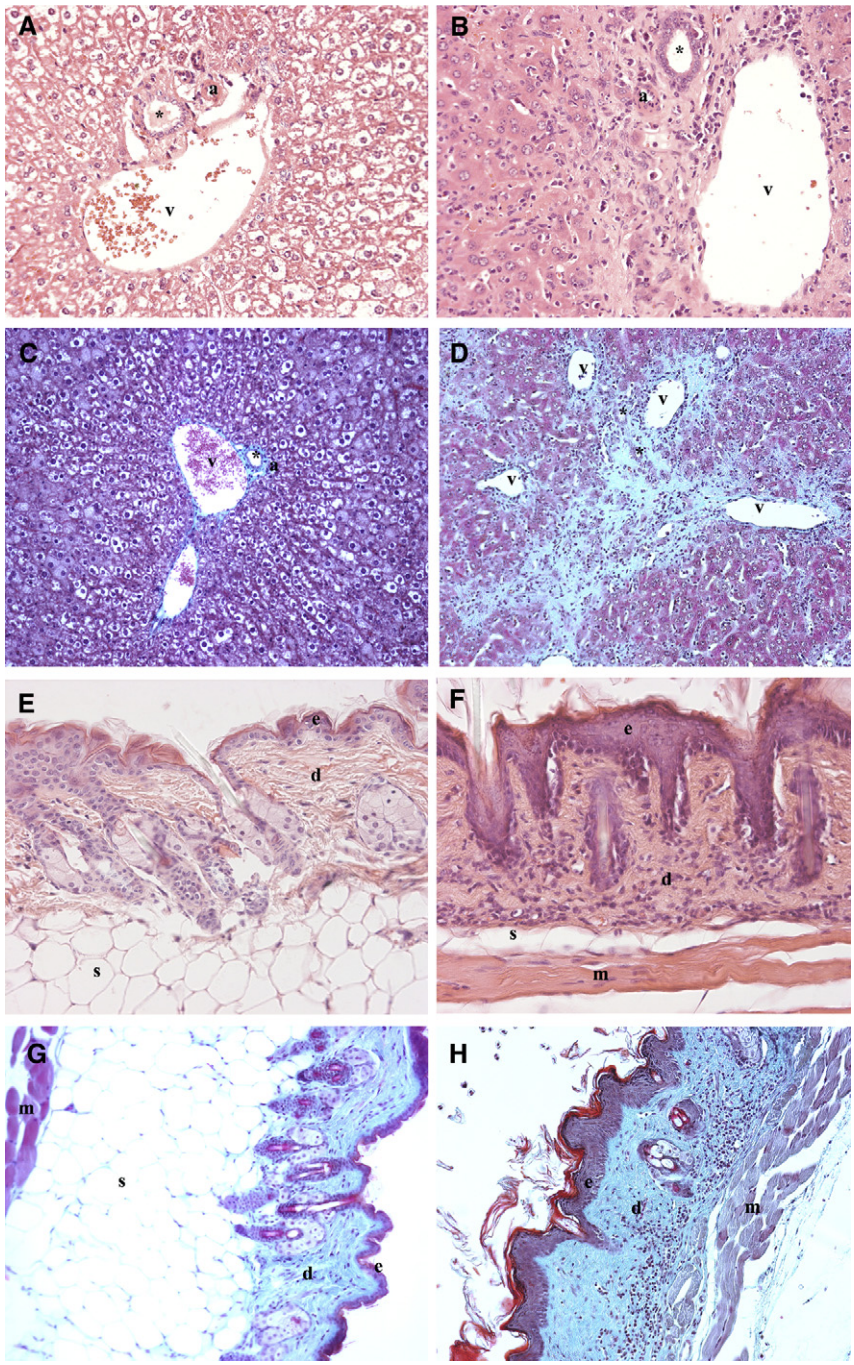

Figure 3. Histological and immunohistochemical analysis of infiltrating human cells in RAG2$^{-/-}\gamma c^{-/-}$ liver and skin. Infiltrate analysis comparing a control mouse with a representative mouse surviving 29 days (liver) and 45 days (skin) after huPBMC injection in experiment 1. The morphology is representative of the observed fibrosis and cell infiltration patterns in a total of 15 examined mice (6 mice in experiment 1 and 9 mice in experiment 2). (A) Normal murine liver, showing no infiltrate or fibrosis in the portal tract (H & E staining; original magnification 20×; control mouse, fibrosis score 0). (B) Liver after injection with human PBMCs, showing infiltration of human cells in the portal tract with extensive fibrosis and an intact bile duct 29 days after huPBMC injection (H & E staining; original magnification 20×; fibrosis score 2). (C) Area corresponding to that shown in (A) demonstrating green staining of collagenous fibers in the hepatic portal area of normal mice (Trichrome staining; original magnification 20×; fibrosis score 0). (D) Area corresponding to that shown in (B) showing extensive collagenous fibrosis (in green) in a mouse injected with huPBMCs (Trichrome staining; original magnification 10×; fibrosis score 2). (E) Normal murine skin, with many hair follicles in the dermis and normal presence of subcutaneous fat (H & E staining; original magnification 20×; control mouse, fibrosis score 0). (F) Skin 45 days after injection with huPBMCs, showing extensive fibrosis of the dermal collagen at the cost of subcutaneous fat and infiltration of human cells subepidermally, perifollicularly, and interstitially (H & E staining; original magnification 20×; fibrosis score 4). (G) Area corresponding to that shown in (E) showing a normal ratio between dermal collagen (green) and subcutaneous fat (Trichrome staining; original magnification, 20×; fibrosis score 0). (H) Area corresponding to that shown in (F) showing extensive collagenous fibrosis (green) in the dermis with a loss of subcutaneous fat (Trichrome staining; original magnification 20×; fibrosis score 4). a, portal artery; v, portal vein; asterisk, bile duct; s, subcutaneous fat; d, dermal tissue; e, epidermal layer; m, muscle.

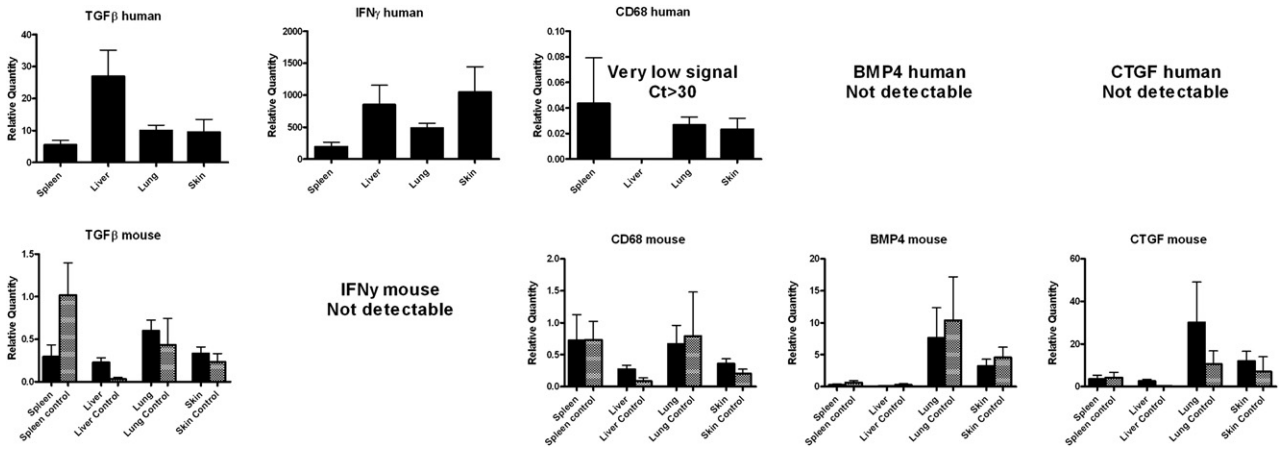

Figure 4. Expression of mRNA for fibrogenic proteins and macrophage markers. Shown is the RQ of RNA for human and murine TGF-β, CD68, BMP4, and CTGF in spleen, lungs, liver, and skin of RAG2$^{-/-}\gamma c^{-/-}$ mice injected with huPBMCs.

DISCUSSION

Here we report for the first time the exact, detailed aspects of sclerotic GVHD in severe immunodeficient RAG2$^{-/-}\gamma c^{-/-}$ mice injected with huPBMCs, with a major focus on the morphology of the damaged organs, infiltration patterns, and molecular aspects of specific cytokines produced in the affected organs. In humans, acute GVHD (aGVHD) is defined based on temporal criteria as a reaction occurring within 100 days posttransplantation, and chronic GVHD (cGVHD) is defined as a reaction developing 100 days or more posttransplantation. A small subset of patients with cGVHD develops a sclerodermatous GVHD (ScGVHD) with fibrotic changes. The time-based distinction between human aGVHD and cGVHD cannot be translated to mouse models, however, because no murine model for GVHD has similar kinetics as humans. Most mouse models demonstrate lethal GVHD within 80 days posttransplantation. This implies that GVHD studies in mice might be better evaluated based on symptomatic similarities to human aGVHD and cGVHD (eg, the ScGVHD subtype), as opposed to time of onset. The distinction between aGVHD and cGVHD in mice is based on predominant T cell subset (Th1 in aGVHD and Th2 in cGVHD) and/or the presence of, for example, autoantibody production and systemic fibrosis [29]. Given our qPCR results showing the presence of both Th1 and Th2 cells, we could not use this as a differentiation criterion in our model. The presence of a systemic fibrotic reaction suggests that in our model, a consistent chronic reaction occurred that appears similar to ScGVHD. Because the mice that we used were immunodeficient, and thus the autoimmune component of human chronic GVHD mediated by autoaggressive T cells emerging from damaged thymus was not seen

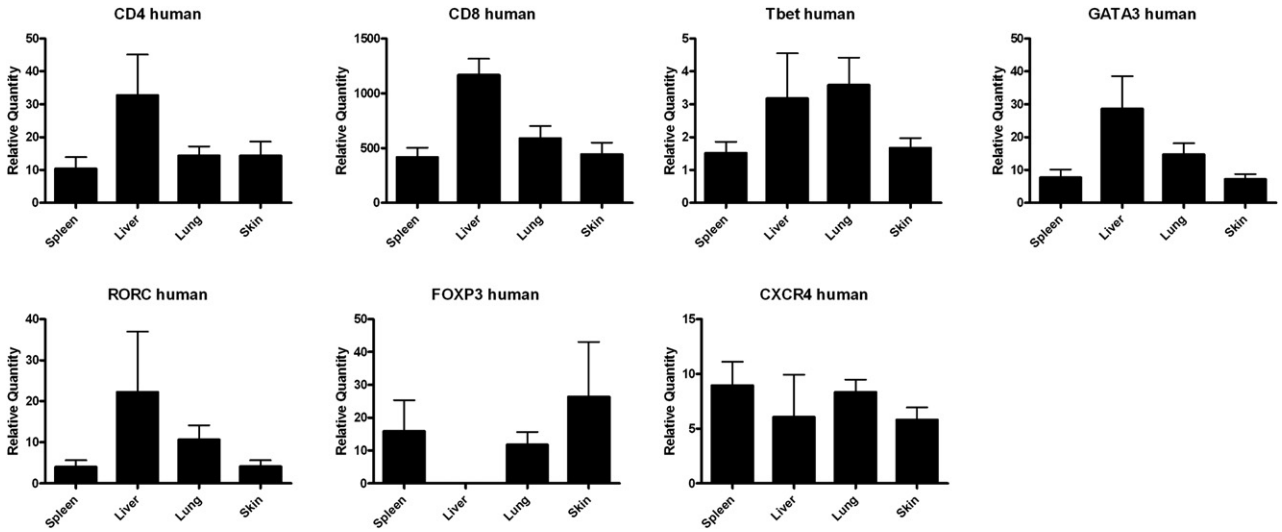

Figure 5. Expression of T cell marker mRNA. Shown is the RQ of RNA for different human cell types, including FoxP3 (Tregs), GATA3 (Th2 cells), Tbet (Th1 cells), RORC (Th17 cells), CD4 (T helper cells), and CD8 (CTLs), including CXCR4 (chemotactin for lymphocytes), in the spleen, lungs, liver, and skin of RAG2$^{-/-}\gamma c^{-/-}$ mice injected with huPBMCs.

in this model, we did not test for the presence of autoantibodies. The sclerotic response in our model is mediated exclusively by mature peripherally derived donor T cells.

Several humanized mouse models, including NOG [21], NOD/SCID [21], NOD/SCID IL2rγ^{null} [29], BALB/cA-RAG2$^{-/-}$IL2r$\gamma^{-/-}$ [21,29], and NOD/SCIDβ2m^{null} [23,29] as well as mouse-mouse models (eg, D10.D2-injected BALB/c mice [30-32]), have been used as models to study the diverse aspects of GVH responses. Those previous studies reported several histological features of a GVH reaction with sclerotic changes, including lung fibrosis [21,23,29,32], skin fibrosis [21,23,30], and fibrotic changes in the liver [21,23,31]. Nevertheless, an exact morphological description of these and other tissues involved in our human-mouse model was lacking. Furthermore, up to now, no specific infiltration patterns for the different human cell phenotypes had been described for xenogeneic mouse models or mouse-mouse models.

In our model, human cells particularly infiltrated the spleen, liver, and lungs. Only low quantities of human cells were detected in the skin, colon, ileum, and kidney, and only sporadic cells were seen in heart valves and bone marrow. This correlates with the known sites of infiltration in previous xenogeneic models [21,23]. The infiltrate showed a mixture of CTLs and T helper cells (including Th1, Th2, and Th17 cells), B cells, and plasma cells, based on immunohistochemistry and qPCR data. The human cells localized in areas that in nonimmunodeficient species would contain lymphoid tissue (ie, spleen and gut); however, in the lungs and liver, the expected bronchial-associated lymphoid tissue was not involved, and infiltrating B cells were often found around blood vessels. The localization of B cells was confined to spleen, lungs and liver. The T cells, including minute amounts of Tregs, were spread diffusely throughout the parenchyma or in the lymphoid origins. Only murine macrophages (mouse CD68$^+$) were found in spleen, liver, lung, skin, and gut, and no human CD68$^+$ macrophages were detected. The organs demonstrated various degrees of fibrosis, with severity correlating with survival time of the mice. Collagenous fibers around blood vessels were detected in almost all cases, and could proliferate and destroy the full architecture of an organ in mice with longer lifespans, correlating with the greater infiltration of human cells in these mice.

As emphasized by Chu et al. [33] in a review of mouse models for GVHD, mouse models might not exactly match or mimic clinical GVHD, but they do illustrate many aspects of the complex mechanism of cGVHD, including ScGVHD, and thus are very useful. Our data show that the morphology of the skin reaction in our model is similar to that described in detail in other mouse-mouse models [30] and xenogeneic models [21,23] and similar to the human skin reaction seen in clinical ScGVHD. This includes the paradox of low human cell infiltrate with nonetheless evident fibrosis. Numerous previous studies have attempted to relate this effect to either CD4$^+$ or CD8$^+$ T cells. Although the GVHD effect in immunodeficient mice is considered to be mediated predominantly by CD4$^+$ cells [34,35], some studies have reported the importance of CD8$^+$ cells in the epidermis in both aGVHD and cGVHD skin biopsy specimens [36] and oral cGVHD [37]. In our humanized mouse model, most T cells were CD8$^+$; however, this does not explain the consequent low cell infiltration. Although T cell infiltration in the skin was low compared with that in the spleen, lungs, and liver, TGF-β and INF-γ production in the skin was not significantly different from that in the spleen and lung. This finding supports the possibility of a direct role of cytokines in inducing tissue damage, as suggested by Dickinson et al. [38], independent of the quantitative amount of human cell infiltrate.

In contrast to human GVHD and other xenogeneic models, the gut of the RAG2$^{-/-}\gamma c^{-/-}$ mice showed no signs of damage, especially no signs of apoptotic colitis, collagen deposition, or any other gastrointestinal features that would normally be expected in human aGVHD and cGVHD. This finding might be related to differences in intestinal bacterial microflora in these specific pathogen-free–bred mice. The intestinal flora is considered to play an important role in fine-tuning the T cell repertoire in gut-associated lymphoid tissue [39], although the exact relationship with GVH response remains unclear.

The pathology in the lung is compatible to that seen in other xenogeneic models and is to some extent comparable to human ScGVHD, in which interstitial fibrosis has been described as a bronchiolitis obliterans pattern [40]; however, instead of being concentrated along bronchioles, it was merely aligned with blood vessels in our mice. In humans, cGVHD in the liver, although rarely biopsied, shows either the classic signs of bile duct epithelial injury with portal lymphocytic infiltration or the hepatic variant with relatively mild bile duct injury and lobular hepatitis [41]. Nevertheless, the loss of bile ducts in human cGVHD might occur only late in the reaction [42,43], and clinical cGVHD may mimic a variety of autoimmune and immunodeficient diseases [33]. The liver morphology in our model did show some resemblance to the histology of human autoimmune hepatitis, including the periportal fibrosis mentioned by Howell et al. [31].

Several cytokines are known to be involved in the GVH reaction, including IFN-γ and TGF-β [44]. Our qPCR data shows production of both human and murine cytokines (Figures 4 and 5). The high levels of TGF-β detected in our model are in line

with the development of fibrosis in general [45-47]. CTGF is a TGF-β–inducible early gene in fibroblasts [48] that interacts directly with BMP4 and TGF-β ligands in extracellular spaces. CTGF has been found to correlate with the formation of sclerosis in scleroderma [49,50], but has not been reported in the context of ScGVHD [51]. In our model, high levels of murine CTGF were detected, which could only have been produced by nonlymphoid murine cells, because the lack of RAG2 and the γc-alleles prevented the formation of murine B cells, T cells, and NK cells. The significantly high levels of human TGF-β could be produced only by human B cells and human T cells, because human macrophages were lacking in our model. Murine TGF-β and BMP4 were elevated in both injected mice and control mice; thus, the high level of TGF-β mRNA cannot be directly related to the development of GVHD by huPBMCs. No expression of other fibrosis-related factors of murine or human origin was detected. Given that IFN-γ may have various functions [52-55], the implications of IFN-γ in our process cannot be easily explained, although it has been related to the fibrosis observed in chronic allograft vasculopathy [56].

The interplay of donor cells and host-derived antigen-presenting cells, to which macrophages belong, and a monocyte-driven fibrotic reaction in the skin was suggested previously [32,33]. Based on our results, we conclude that there must be interplay among human B cells and T cells and mouse macrophages at the level of human TGF-β and INF-γ with murine CTGF, resulting in the formation of fibrosis.

Despite some differences with human cGVHD, more specifically the human ScGVHD subtype, we must agree with Chu et al. [33] and Schroeder et al. [29] that mouse models are crucial for GVHD studies, although the mouse model must be chosen wisely, based on the targets of interest. Apart from differences in GVH phenotype in various mouse strains (and even in the same model for GVH response), the outcome of the induced reaction often depends on conditioning regimen, irradiation dose, donor source, and even age of the mice undergoing transplantation [29]. In our experiments, the level of human chimerism varied, and some variation was observed when comparing the scores of the histological or immunohistochemical evaluation for significance. Nevertheless, we detected a consistent pattern, either significant or at least as a trend, for both morphology and migration in our human-mouse model. Thus, we consider detailed histopathological features, including the similarities and differences between mouse models and human cGVHD (more specifically, ScGVHD), an absolute necessity for future studies of GVHD.

In conclusion, our histological, immunohistochemical, and molecular analyses of the ScGVHD in the RAG2$^{-/-}\gamma c^{-/-}$ mouse have established this human-mouse model as relevant for the study of ScGVHD and has enabled us to examined the various processes involved in GVHD caused by either donor or recipient cells. This opens the possibility of studying specific therapeutic approaches directed at either of these processes using reagents directed to either mouse or human targets.

ACKNOWLEDGMENTS

Authorship Statement: Marieke C. H. Hogenes and Roel A. de Weger designed the study. Marieke C. H. Hogenes, Suzanne van Dorp, Joyce van Kuik, Filipa R. P. Monteiro, Natalie ter Hoeve, and Anton C. Martens conducted research, including the clinical part of the experiment, histopathological techniques, and molecular analysis. Marieke C. H. Hogenes, Joyce van Kuik, Marijke R. van Dijk, and Roel A. de Weger evaluated the histology, immunohistochemical and molecular data. Joyce van Kuik performed the molecular analyses. Marieke C. H. Hogenes, Joyce van Kuik, Marijke R. van Dijk, and Roel A. de Weger analyzed and interpreted the results. Marieke C. H. Hogenes, Joyce van Kuik, Anton C. Martens, and Roel A. de Weger wrote the manuscript. All authors reviewed the final draft of the manuscript.

Financial disclosure: The authors have no conflicts of interest to disclose.

SUPPLEMENTARY DATA

Supplementary data related to this article can be found online at doi:10.1016/j.bbmt.2012.05.002

REFERENCES

1. Farag SS. Chronic graft-versus-host disease: where do we go from here? *Bone Marrow Transplant*. 2004;33:569-577.
2. Ferrara J, Antin J. The pathophysiology of graft-vs-host disease. In: Blume KG, editor. *Thomas' Hematopoietic Cell Transplantation*. Malden, MA: Blackwell Science; 2004. p. 353-368.
3. Lee SJ. New approaches for preventing and treating chronic graft-versus-host disease. *Blood*. 2005;105:4200-4206.
4. Canninga-van Dijk MR, van der Straaten HM, Fijnheer R, et al. Anti-CD20 monoclonal antibody treatment in 6 patients with therapy-refractory chronic graft-versus-host disease. *Blood*. 2004;104:2603-2606.
5. Dazzi F, Marelli-Berg FM. Mesenchymal stem cells for graft-versus-host disease: close encounters with T cells. *Eur J Immunol*. 2008;38:1479-1482.
6. Liotta F, Frosali F, Querci V, et al. Human immature myeloid dendritic cells trigger a TH2-polarizing program via Jagged-1/Notch interaction. *J Allergy Clin Immunol*. 2008;121:1000-1005.
7. Maccario R, Podesta M, Moretta A, et al. Interaction of human mesenchymal stem cells with cells involved in alloantigen-specific immune response favors the differentiation of $CD4^+$ T-cell subsets expressing a regulatory/suppressive phenotype. *Haematologica*. 2005;90:516-525.
8. Ramasamy R, Tong CK, Seow HF, et al. The immunosuppressive effects of human bone marrow–derived mesenchymal stem cells target T cell proliferation but not its effector function. *Cell Immunol*. 2008;251:131-136.

9. Shimabukuro-Vornhagen A, Hallek MJ, Storb RF, et al. The role of B cells in the pathogenesis of graft-versus-host disease. *Blood*. 2009;114:4919-4927.
10. Zhen Y, Zheng J, Zhao Y. Regulatory $CD4^+CD25^+$ T cells and macrophages: communication between two regulators of effector T cells. *Inflamm Res*. 2008;57:564-570.
11. Berney T, Molano RD, Pileggi A, et al. Patterns of engraftment in different strains of immunodeficient mice reconstituted with human peripheral blood lymphocytes. *Transplantation*. 2001; 72:133-140.
12. Goldman JP, Blundell MP, Lopes L, et al. Enhanced human cell engraftment in mice deficient in RAG2 and the common cytokine receptor gamma chain. *Br J Haematol*. 1998;103:335-342.
13. Lubin I, Segall H, Marcus H, et al. Engraftment of human peripheral blood lymphocytes in normal strains of mice. *Blood*. 1994;83:2368-2381.
14. Mosier DE, Gulizia RJ, Baird SM, et al. Transfer of a functional human immune system to mice with severe combined immunodeficiency. *Nature*. 1988;335:256-259.
15. van Rijn RS, Simonetti ER, Hagenbeek A, et al. A new xenograft model for graft-versus-host disease by intravenous transfer of human peripheral blood mononuclear cells in $RAG2^{-/-}\gamma^{-/-}$ double-mutant mice. *Blood*. 2003;102:2522-2531.
16. Ishikawa F, Yasukawa M, Lyons B, et al. Development of functional human blood and immune systems in NOD/SCID/IL2 receptor γ $chain^{null}$ mice. *Blood*. 2005;106:1565-1573.
17. McCune JM, Namikawa R, Kaneshima H, et al. The SCID-hu mouse: murine model for the analysis of human hematolymphoid differentiation and function. *Science*. 1988;241:1632-1639.
18. McDermott SP, Eppert K, Lechman ER, et al. Comparison of human cord blood engraftment between immunocompromised mouse strains. *Blood.* XXXX;116:193–200.
19. Shultz LD, Lyons BL, Burzenski LM, et al. Human lymphoid and myeloid cell development in NOD/LtSz-*scid IL2R*γ^{null} mice engrafted with mobilized human hemopoietic stem cells. *J Immunol*. 2005;174:6477-6489.
20. Tary-Lehmann M, Saxon A, Lehmann PV. The human immune system in hu-PBL-SCID mice. *Immunol Today*. 1995;16:529-533.
21. Ito R, Katano I, Kawai K, et al. Highly sensitive model for xenogenic GVHD using severe immunodeficient NOG mice. *Transplantation*. 2009;87:1654-1658.
22. King MA, Covassin L, Brehm MA, et al. Human peripheral blood leucocyte non-obese diabetic-severe combined immunodeficiency interleukin-2 receptor γ chain gene mouse model of xenogeneic graft-versus-host–like disease and the role of host major histocompatibility complex. *Clin Exp Immunol*. 2009; 157:104-118.
23. Nervi B, Rettig MP, Ritchey JK, et al. Factors affecting human T cell engraftment, trafficking, and associated xenogeneic graft-vs-host disease in NOD/SCID $\beta 2m^{null}$ mice. *Exp Hematol*. 2007;35: 1823-1838.
24. Hesselton RM, Koup RA, Cromwell MA, et al. Human peripheral blood xenografts in the SCID mouse: characterization of immunologic reconstitution. *J Infect Dis*. 1993;168:630-640.
25. Hoffmann-Fezer G, Gall C, Zengerle U, et al. Immunohistology and immunocytology of human T-cell chimerism and graft-versus-host disease in SCID mice. *Blood*. 1993;81:3440-3448.
26. Weijer K, Uittenbogaart CH, Voordouw A, et al. Intrathymic and extrathymic development of human plasmacytoid dendritic cell precursors in vivo. *Blood*. 2002;99:2752-2759.
27. Hagemeijer MC, van Oosterhout MF, van Wichen DF, et al. T cells in cardiac allograft vasculopathy are skewed to memory Th-1 cells in the presence of a distinct Th-2 population. *Am J Transplant*. 2008;8:1040-1050.
28. Fast LD, DiLeone G, Cardarelli G, et al. Mirasol PRT treatment of donor white blood cells prevents the development of xenogeneic graft-versus-host disease in $Rag2^{-/-}\gamma c^{-/-}$ double-knockout mice. *Transfusion*. 2006;46:1553-1560.
29. Schroeder MA, DiPersio JF. Mouse models of graft-versus-host disease: advances and limitations. *Dis Model Mech*. 2011;4: 318-333.
30. Claman HN, Jaffee BD, Huff JC, et al. Chronic graft-versus-host disease as a model for scleroderma, II: mast cell depletion with deposition of immunoglobulins in the skin and fibrosis. *Cell Immunol*. 1985;94:73-84.
31. Howell CD, Yoder T, Claman HN, et al. Hepatic homing of mononuclear inflammatory cells isolated during murine chronic graft-vs-host disease. *J Immunol*. 1989;143:476-483.
32. McCormick LL, Zhang Y, Tootell E, et al. Anti–TGF-β treatment prevents skin and lung fibrosis in murine sclerodermatous graft-versus-host disease: a model for human scleroderma. *J Immunol*. 1999;163:5693-5699.
33. Chu YW, Gress RE. Murine models of chronic graft-versus-host disease: insights and unresolved issues. *Biol Blood Marrow Transplant*. 2008;14:365-378.
34. Contassot E, Murphy W, Angonin R, et al. In vivo alloreactive potential of ex vivo–expanded primary T lymphocytes. *Transplantation*. 1998;65:1365-1370.
35. Ferrara JL. Cytokines and the regulation of tolerance. *J Clin Invest*. 2000;105:1043-1044.
36. Favre A, Cerri A, Bacigalupo A, et al. Immunohistochemical study of skin lesions in acute and chronic graft-versus-host disease following bone marrow transplantation. *Am J Surg Pathol*. 1997;21:23-34.
37. Imanguli MM, Swaim WD, League SC, et al. Increased T-bet^+ cytotoxic effectors and type I interferon–mediated processes in chronic graft-versus-host disease of the oral mucosa. *Blood*. 2009;113:3620-3630.
38. Dickinson AM, Sviland L, Dunn J, et al. Demonstration of direct involvement of cytokines in graft-versus-host reactions using an in vitro human skin explant model. *Bone Marrow Transplant*. 1991;7:209-216.
39. Sawamura SA, Tanaka K, Noda S, et al. The role of intestinal bacterial flora in the tuning of the T cell repertoire. *Immunobiology*. 1999;201:120-132.
40. Wolff D, Reichenberger F, Steiner B, et al. Progressive interstitial fibrosis of the lung in sclerodermoid chronic graft-versus-host disease. *Bone Marrow Transplant*. 2002;29:357-360.
41. Akpek G, Boitnott JK, Lee LA, et al. Hepatitic variant of graft-versus-host disease after donor lymphocyte infusion. *Blood*. 2002;100:3903-3907.
42. Andersen CB, Horn T, Sehested M, et al. Graft-versus-host disease: liver morphology and pheno/genotypes of inflammatory cells and target cells in sex-mismatched allogeneic bone marrow transplant patients. *Transplant Proc*. 1993;25(1 Pt 2): 1250-1254.
43. Yeh KH, Hsieh HC, Tang JL, et al. Severe isolated acute hepatic graft-versus-host disease with vanishing bile duct syndrome. *Bone Marrow Transplant*. 1994;14:319-321.
44. Deeg HJ. Cytokines in graft-versus-host disease and the graft-versus-leukemia reaction. *Int J Hematol*. 2001;74:26-32.
45. Ihn H, Yamane K, Kubo M, et al. Blockade of endogenous transforming growth factor β signaling prevents up-regulated collagen synthesis in scleroderma fibroblasts: association with increased expression of transforming growth factor β receptors. *Arthritis Rheum*. 2001;44:474-480.
46. Kubo M, Ihn H, Yamane K, et al. Up-regulated expression of transforming growth factor β receptors in dermal fibroblasts in skin sections from patients with localized scleroderma. *Arthritis Rheum*. 2001;44:731-734.
47. Del Galdo F, Jimenez SA. T cells expressing allograft inflammatory factor 1 display increased chemotaxis and induce a profibrotic phenotype in normal fibroblasts in vitro. *Arthritis Rheum*. 2007;56:3478-3488.
48. Zhang Y, McCormick LL, Gilliam AC. Latency-associated peptide prevents skin fibrosis in murine sclerodermatous graft-versus-host disease, a model for human scleroderma. *J Invest Dermatol*. 2003;121:713-719.
49. Igarashi A, Nashiro K, Kikuchi K, et al. Connective tissue growth factor gene expression in tissue sections from localized scleroderma, keloid, and other fibrotic skin disorders. *J Invest Dermatol*. 1996;106:729-733.

50. Igarashi A, Nashiro K, Kikuchi K, et al. Significant correlation between connective tissue growth factor gene expression and skin sclerosis in tissue sections from patients with systemic sclerosis. *J Invest Dermatol*. 1995;105:280-284.
51. Wu JM, Thoburn CJ, Wisell J, et al. CD20, AIF-1, and TGF-β in graft-versus-host disease: a study of mRNA expression in histologically matched skin biopsies. *Mod Pathol*. 2010;23: 720-728.
52. Murphy WJ, Welniak LA, Taub DD, et al. Differential effects of the absence of interferon-γ and IL-4 in acute graft-versus-host disease after allogeneic bone marrow transplantation in mice. *J Clin Invest*. 1998;102:1742-1748.
53. del Rosario ML, Zucali JR, Kao KJ. Prevention of graft-versus-host disease by induction of immune tolerance with ultraviolet B-irradiated leukocytes in H-2 disparate bone marrow donor. *Blood*. 1999;93:3558-3564.
54. Brok HP, Vossen JM, Heidt PJ. IFN-γ–mediated prevention of graft-versus-host disease: pharmacodynamic studies and influence on proliferative capacity of chimeric spleen cells. *Bone Marrow Transplant*. 1998;22:1005-1010.
55. Yang YG, Sergio JJ, Pearson DA, et al. Interleukin-12 preserves the graft-versus-leukemia effect of allogeneic CD8 T cells while inhibiting CD4-dependent graft-versus-host disease in mice. *Blood*. 1997;90:4651-4660.
56. Yi T, Rao DA, Tang PC, et al. Amelioration of human allograft arterial injury by atorvastatin or simvastatin correlates with reduction of interferon-γ production by infiltrating T cells. *Transplantation*. 2008;86:719-727.